Journal of Molecular Catalysis A: Chemical 333 (2010) 136–144

Contents lists available at ScienceDirect

Journal of Molecular Catalysis A: Chemical

journal homepage: www.elsevier.com/locate/molcata

Hydrogenolysis of hydroxymatairesinol on Y derived catalysts: A computational study

Giampaolo Barone[a], Giovanni Li Manni[a,1], Antonio Prestianni[a], Dario Duca[a,*], Heidi Bernas[b], Dmitry Yu. Murzin[b]

[a] Dipartimento di Chimica Inorganica e Analitica "Stanislao Cannizzaro" Universitá di Palermo, viale delle Scienze Ed. 17, I-90128 Palermo, Italy
[b] Laboratory of Industrial Chemistry, Process Chemistry Centre, Åbo Akademi University, Biskopsgatan 8, FIN-20500 Turku, Finland

ARTICLE INFO

Article history:
Received 24 June 2010
Received in revised form
28 September 2010
Accepted 7 October 2010
Available online 17 October 2010

Keywords:
7-Hydroxymatairesinol
Hydrogenation/dehydration processes
H-Y zeolite
Supported catalysts
DFT calculations

ABSTRACT

Hydrogenolysis of 7-hydroxymatairesinol (HMR) to matairesinol (MAT) occurs on palladium supported acidic catalysts. HMR has three stereochemical centres and naturally exists as a mixture of two diastereoisomers, namely RRR-HMR and SRR-HMR. The latter is significantly more reactive than the former, in the reaction above. In order to elucidate the hydrogenolysis mechanism, simple surface events involving HMR derivatives on aluminated faujasite (H-Y) fragments were simulated by quantum chemical calculations. The metallic function of a Pd/H-Y acidic catalyst was also mimicked by a minimal palladium cluster. Stereochemical evidences pointed already out that water β-elimination on the epimeric centre, leading to an olefinic intermediate, should mainly occur for the adsorbed SRR-HMR stereoisomer. As a consequence, it was hypothesized that this feature could explain the different reactivity of the RRR-HMR and SRR-HMR hydrogenolysis, occurring on metal supported bi-functional zeolite catalysts. The significance of this inference is decreased by the here study. Finally, it is demonstrated that several HMR to MAT reaction paths may coexist and that the metal component of the Pd/H-Y bi-functional catalyst cannot be involved in steps discriminating for the whole reaction rate and selectivity.

1. Introduction

Matairesinol (MAT) is a substance showing interesting biological properties. It has antioxidative and preventive effects against hormone-dependent cancers – such as breast, prostate, and colon cancers – and it helps to maintain a good cardiovascular health [1–3]. MAT can be obtained by hydrogenolysis of the natural product 7-hydroxymatairesinol (HMR, see Fig. 1) also over palladium catalyst supported on acidic zeolite.

HMR is a member of the lignans, defined as a class of phenolic compounds possessing a 2,3-dibenzylbutane skeleton. HMR is abundant in the knots of the Norway spruce (Picea abies) [4–6] and exists in nature as a mixture of two diastereisomers: the (7R,8R,8′R)-(-)-7-allo-hydroxymatairesinol (RRR-HMR), which is the less abundant isomer, and the (7S,8R,8′R)-(-)-7-hydroxymatairesinol (SRR-HMR) [7,8]. The isomers differ for the chirality around the C7 atom.

Experimental studies [9–13] on the title hydrogenolysis, performed over supported palladium catalysts, pointed out that: (i) Brønsted acidic sites are necessary for the reaction and palladium on SiO_2 and Al_2O_3 is in fact not active, (ii) conversion of HMR to MAT increases with the number of the Brønsted acidic sites for the carbon supported catalysts but decreases with the number of the same acidic sites for the zeolite supported catalysts, (iii) SRR isomer reacts about three times faster than RRR isomer, (iv) at the same time, SRR-HMR easily isomerizes to RRR-HMR and finally (v) the reaction product is mainly constituted by the RR-MAT isomer.

Moreover, it has been also observed that the conversion of HMR to MAT occurring on palladium supported on aluminated faujasite (H-Y) is ca. 95%, with a selectivity to MAT of 92%, while using palladium supported on aluminated ZSM-5 zeolites (H-ZSM-5) the conversion is only 5%, after 4 h [11]. This finding might be explained by considering that HMR is too large to pass through the small pores of H-ZSM-5, and by inferring that the small conversion observed on the Pd/H-ZSM-5 system should take place mainly on the catalytic sites of the external surface. Conversely, pores and cavities of H-Y should be large enough to allow diffusion and adsorption of HMR hence its conversion to MAT. Although this explanation easily accounts for the local reaction sensitivity and namely for the different conversion rate and conversion percentage, occurring on H-Y and H-ZSM-5, there is not yet a simple explanation of the whole

* Corresponding author. Tel.: +39 091 489714; fax: +39 091 427584.
E-mail address: dduca@cccp.unipa.it (D. Duca).
[1] Present address: Department of Physical Chemistry, Geneva University, Switzerland.

1381-1169/$ – see front matter © 2010 Elsevier B.V. All rights reserved.
doi:10.1016/j.molcata.2010.10.010

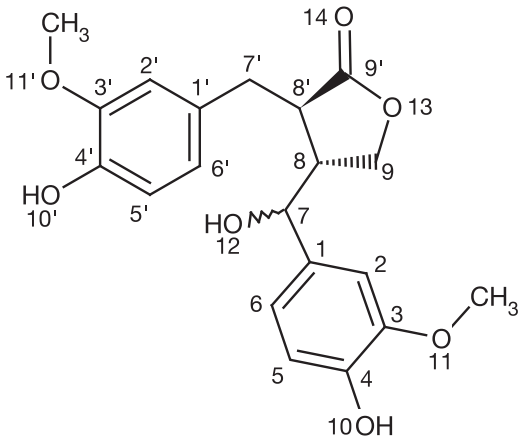

Fig. 1. Schematic representation of 7-hydroxymatairesinol (HMR): structure and numbering.

reactivity observed on differently supported palladium catalysts for the SRR-HMR and the RRR-HMR diastereoisomers.

The proposed HMR hydrogenolysis mechanism (M1) is reported in Fig. 2 [10]. The M1 reaction mechanism involves: (i) the protonation of the –OH12 group with consequent water-elimination, followed by (ii) hydride addition to the carbenium ionic species to produce MAT. It has to be emphasized that in M1, the water-elimination step induces loss of chirality into the epimeric C7 centre, discriminating between RRR and SRR isomers. As a consequence, the different reaction rates observed for the two HMR isomers could be ascribed, as recently hypothesized [12,13], to an equilibrium, occurring between the same isomers.

However, the observed reactivity could also be related to the conformational flexibility of the HMR molecule, mainly determined by the rotations of the dihedral angles around the C1–C7, C7–C8, C1′–C7′ and C7′–C8′ bonds (see Fig. 1). In particular, because of its size and flexibility, HMR may easily assume different conformations that could independently interact with the adsorption sites of the supported metal catalyst. These considerations have recently prompted us to perform a systematic conformational analysis of the two HMR epimers and to individually investigate the energetic and structural properties of their most stable conformer as well as of their protonated and olefinic intermediates [14]. In the study above, we have considered two intermediate species as originated by the HMR epimers. The first, already proposed in the M1 mechanism, involves the protonation of the benzylic oxygen, i.e. the –OH12 group, giving the carbenium ionic species. The second, shown in Fig. 3, is an olefinic intermediate formed by a different mechanism (M2), as explained below.

The conformational results concerning the RRR-HMR and the SRR-HMR diasteroisomers showed that three typical conformational families – with open, semi-folded and folded structure – can be obtained. The three families displayed small structural differences [14], mainly involving the relative orientations of the –OH and $-OCH_3$ groups 10, 11, 10′ and 11′ (see Fig. 1). These findings allowed us to propose, by stereochemical considerations, a possible explanation of the higher reactivity of the SRR with respect to the RRR isomer, when hydrogenolysis is catalyzed by palladium supported either on acidic zeolite or on carbonaceous material [14].

It was indeed observed that although the most stable conformers of SRR-HMR and RRR-HMR possess roughly the same energy content, the mutual disposition of the H8 atom and of the –OH12 group is different (see Fig. 4), being in *syn* and in *anti* conformation in the SRR and in the RRR epimers, respectively. These conforma-

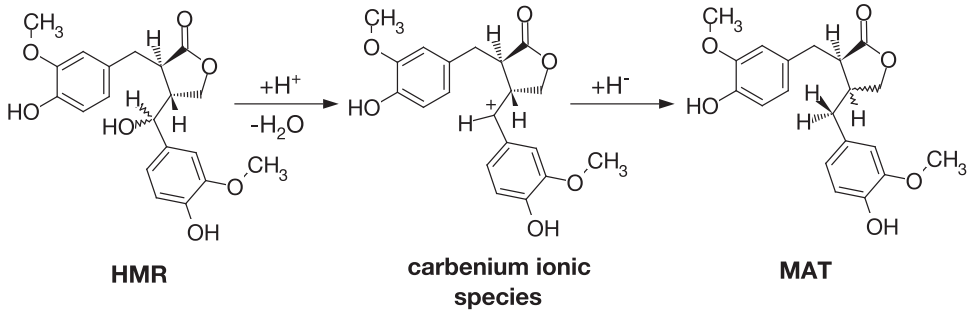

Fig. 2. Schematic representation of the HMR to MAT–M1–reaction mechanism: one carbenium species is involved.

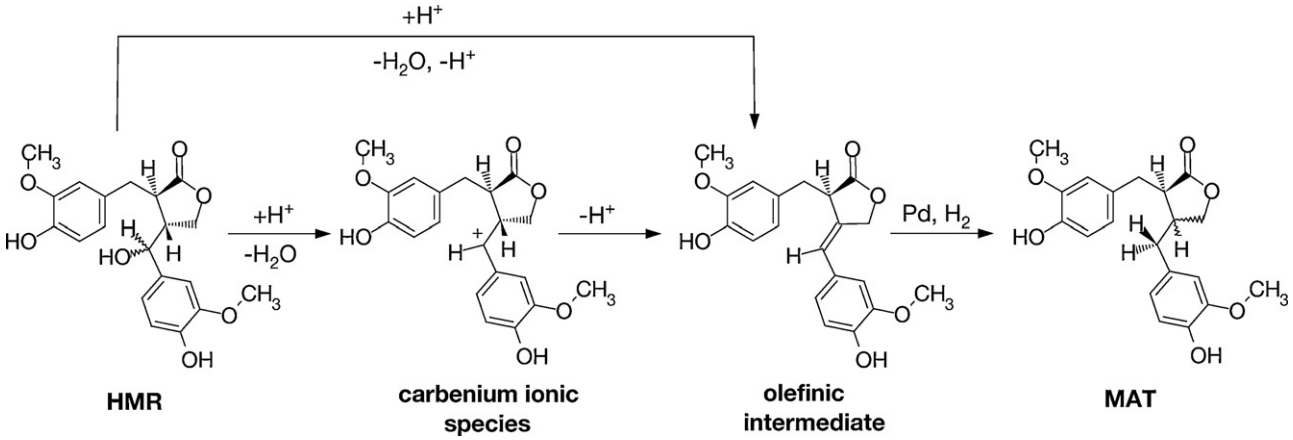

Fig. 3. Schematic representation of the HMR to MAT–M2–reaction mechanism: M2 is devised by two pathways, M2a and M2b; the first at variance with the second involves the formation of the carbenium ionic species.

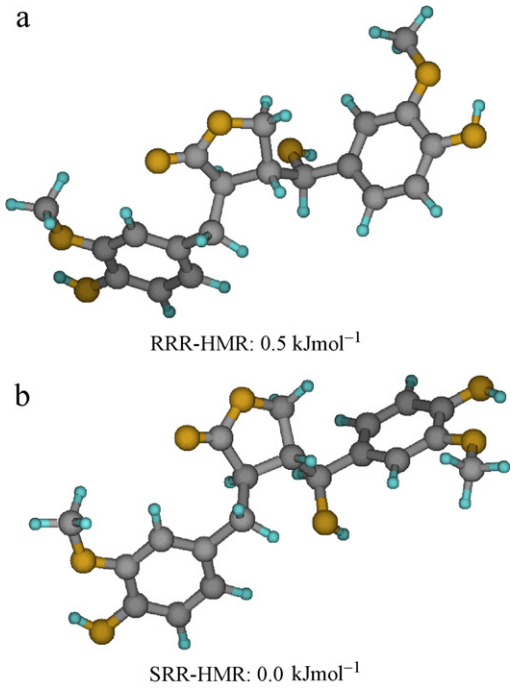

Fig. 4. Optimized geometry of the most stable conformers found for the RRR (4a) and SRR (4b) epimers of HMR; the relative standard free energy values calculated in ethanol solution for the 2 epimers [14] are reported below the corresponding isomer structures.

tions, affecting the substrate/catalyst interactions, could actually account for the different kinetics of the two epimers.

In fact, beside M1, two alternative reaction pathways (M2a and M2b, see Fig. 3) can be hypothesized when hydrogenolysis of hydroxymatairesinol occurs on catalysts that, as the acidic zeolite supported catalysts, show both acidic and nucleophilic sites [14]. M2a and M2b can be regarded like two pathways, which form the M2 mechanism, alternative to the M1 mechanism summarized in Fig. 2. In the M2a pathway, after the protonation water-elimination step, the deprotonation of the H8 atom – taking place through a two steps β-elimination (i.e OH_2 followed by H^+, E1 removals) – could give rise to the formation of an olefinic intermediate, which after the reduction of the double bond, for example addressed by supported palladium in presence of adsorbed hydrogen, could produce MAT. In this respect, the presence of the supported metallic function would be needed for reducing the olefinic intermediate. The M2a pathway can be invoked for both the RRR and SRR epimers. The M2b pathway consists in a E2 β-elimination for a concerted deprotonation water-elimination step. It can occur mainly, if not exclusively, for the SRR epimer, giving rise to the olefinic intermediate without formation of the carbenium ion, due to the *syn* conformation of its H8 atom and of –OH12 group that simultaneously face on eventually present contiguous acidic and nucleophilic sites of the catalyst surface [14].

The feasibility and the role of the whole M2 mechanism as well as its connection with the M1 mechanism has been investigated in this work. To this aim, we have considered the interactions of the two HMR epimers and of their derivatives (i.e. carbenium and olefinic species as well as the product) with a 48T [15] H-Y fragment.

Several computational chemistry methods have been advised and applied for the investigation of the zeolite properties and of their role in the reactivity of small organic molecules. A short selection of recent publications on the theoretical treatment of zeolite based catalysis, either of interest for the present work or useful for individuating the seminal papers on the subject, is

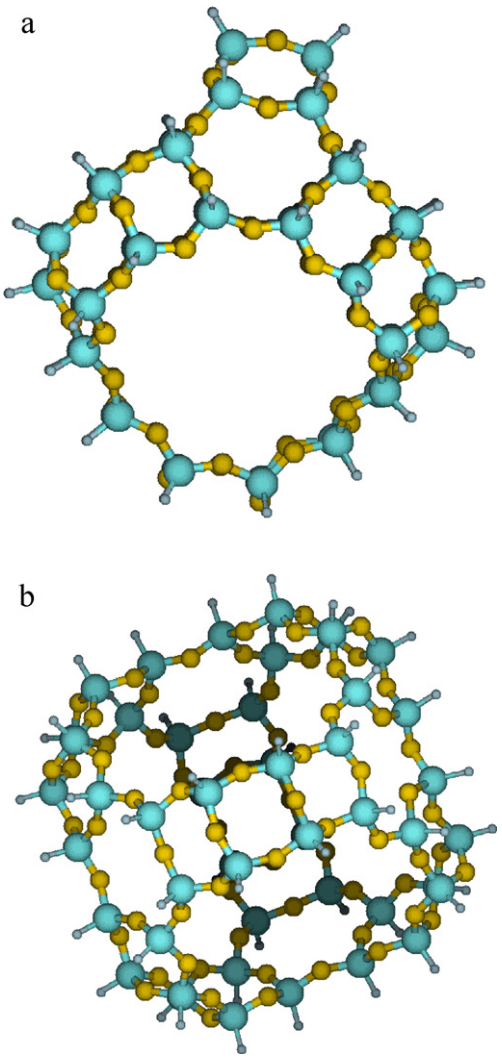

Fig. 5. Two different views of the faujasite fragment, used as model.

here outlined [16–19]. Concerning the same application field, we have recently reported on DFT investigations taking into consideration the adsorption and reactivity of small organic species within acidic zeolite cavities also in the presence of embedded Pd atoms [15,20,21], using the cluster approach [22].

Our study, presented from the methodological point of view in the Computational details and analyzed in Section 3, is arranged as follows. The protonation, water-elimination, deprotonation and hydrogenation steps catalyzed by the H-Y acidic zeolite model to produce the carbenium and the olefinic intermediates or the MAT species were investigated, by studying the interaction between both the HMR epimers and their derivatives with a highly symmetric and sizable fragment of the H-Y zeolite. Whereas, to mimic the role of the metal in the bi-functional Pd/H-Y catalyst, the hydrogenation kinetics over a minimal hydrogenated palladium cluster ($2H/Pd_2$) were studied, involving either the olefinic or the carbenium species that were previously produced on the H-Y fragment.

Topics of the present work are in our opinion also stimulating in view of the recent interest in replacing oil, in the petrochemical industry, with other feedstocks, including derived from biomass [23]. In fact, a lot of efforts is at present dedicated to the transformation processes of polyols. The task is to remove oxygen from –OH groups also in secondary alcohols, e.g. carbohydrates, lignins and lignans, through hydrogenolysis in the presence of metallic

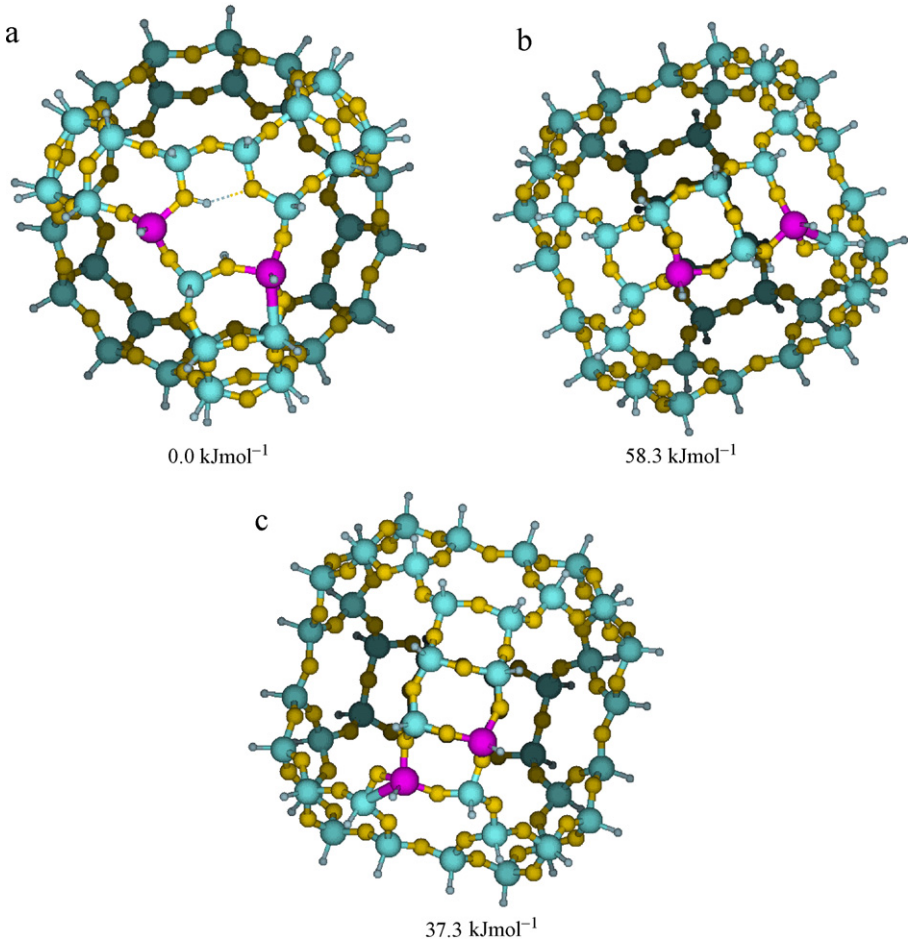

Fig. 6. Views of three different H-Y cavities characterized by different placements of the aluminum and acidic hydrogen centres; the relative DFT energy values are indicated below the corresponding fragment; in the fragment (6a) both the aluminum atoms are placed in a 6T ring, in the (6b) on a 6T ring and on a non-adjacent 4T ring and finally in the (6c) on a 6T ring and on an adjacent 4T ring.

and acidic sites. Thus, the here HMR case represents an interesting example, whose results and concepts can be useful for designing other similar processes, when the corresponding reaction pathways include catalytic dehydration/hydrogenation steps.

2. Computational details

The Gaussian 03 (G03) suite of programs was used for all the calculations performed in the present work [24]. The considered Y model is a 48T fragment corresponding to the super cage of faujasite (see Fig. 5). The fragment has been extracted from a DLS refined X-ray structure [25–27] and it is formed by 168 atoms, among which 48 are external (capping) hydrogen atoms, added as cut-off points [15,20,21]. The coordinates of the capping hydrogen atoms were initially optimized by DFT approaches at B3LYP/3-21G level, fixing the positions of the remaining atoms; then, the full structure was re-optimized at B3LYP/3-21G level, fixing the positions of the H atoms [21]. The so obtained fragment was after used as starting moiety for following optimizations.

The selected Y model, is characterized by an incoming pore size of about 1200 pm and a diameter of the super cage of about 1500 pm. In the cavity model there are only two kinds of Si sites, i.e. those forming 6T and 4T rings. In this model, two aluminum atoms substituted two silicon atoms to reproduce the acidic (H-Y) system. Two protons on different oxygen atoms, surrounding the aluminum sites and pointing toward the super cage room of the zeolite, were introduced to neutralize the negative charges originated by the substitution of the aluminum atoms [15,20,21].

In order to establish the most stable acidic configuration, several structures (see Fig. 6) differing for the position of the aluminum and of the acidic hydrogen sites were generated. In the different structures, the aluminum atoms were each other close but not contiguous, according to the Loewenstein rule [28]. In the most stable structure (see Fig. 6a) one proton was eliminated to generate, contiguously to the surface acidic site, a nucleophilic centre. The latter was introduced in that position to allow simultaneous interactions of one nucleophilic and one acidic centre of the zeolite with the β-hydrogen, H8, and the hydroxyl group, –OH12, of the HMR species.

Due to the large size of the H-Y zeolite models, hence to keep the computing cost at reasonable levels, the standard 6-31G(d,p) basis set was employed to describe the vicinal 3T ($H_4Al_2SiO_7$) moiety including both the aluminum atoms and the silicon in-between (see Fig. 6a), while the 3-21G basis set was employed to describe the remaining atoms of the zeolite framework. Indeed, it has been recently reported that the combination of the 3-21G and 6-31G(d,p) basis sets – employed to study structures as well as differential energetics and kinetics of zeolite systems – is able to give structural and differential energy results comparable to those obtained by using either 6-31G(d,p) or 6-311+G(2d,2p) basis sets for all the zeolite atoms [20].

The 6-31G(d,p) basis set was also used to describe the HMR species adsorbed within the zeolite cavity and the corresponding derivatives, occurring along the HMR reaction to MAT. Furthermore, the same pathway in confined space was also investigated by two layers ONIOM calculations [29,30], using the B3LYP/6-

31G(d,p) method for the higher level (high-level) layer and the semiempirical AM1 method [31] for the lower level (low-level) layer.

Aim of such calculations was to characterize the stationary points found by DFT in terms of energy minima or transition state (TS) structures, as well as to evaluate their standard free energy values [32]. The HMR molecules and their derivatives, together with the 3T moiety containing both the Al atoms, were always included in the high-level layer. Since the partial geometry optimizations were performed fixing the coordinates of the capping hydrogen atoms, spurious imaginary frequencies were regularly observed. In those cases, however, it was always possible to find out the imaginary frequencies attributable to the reaction coordinates. In passing, it is also recalled that error cancellations were expected when calculating relative values of standard free energy for the systems whose geometries were optimized at the same level of theory, using the same constrains [15].

Second-order Møller–Plesset (MP2) [33] perturbation theory calculations – as standardly implemented in the G03 program package [34–37] – were carried out on the HMR hydrogenolysis derivatives, using the 6-31G(d,p) basis set for all the atoms, with the exception of the capping hydrogens, that were treated by the 3-21G basis set. These calculations were performed in order to check the presence of possible dispersion (dipolar) effects [17,19] exerted by the zeolite framework on HMR and its derivatives, when located inside the H-Y fragments.

The kinetics of the reduction of both olefinic and carbenium species, over a $2H/Pd_2$ cluster, used as model of the hydrogenated palladium component of the bi-functional catalyst, were also analyzed by the B3LYP method. The Los Alamos ECP basis set was used for the Pd atoms and the 6-31G(d,p) basis set for the other atoms (H, C, O) [20]. Only the singlet spin states (corresponding to the most stable states) were considered for the different systems analyzed. Energy and structure of the transition states were obtained using the transit-guided quasi-Newton method [38]. Vibration frequency analyses, within the harmonic approximation, were performed on the geometries optimized by the ONIOM method, to confirm whether they represented a TS or a minimum in the potential energy surface [32], while the zero point energy (ZPE) correction was applied in the energetic evaluations.

3. Results and discussion

As detailed in the preceding section, two aluminum atoms substituted two silicon atoms in different positions (see Fig. 6). The structure reported in Fig. 6a is the most stable, presumably because one of the two protons is positioned at the centre of a 6T ring, interacting with oxygen atoms of the same ring. Conversely, in the structures reported in Fig. 6b and c both protons point toward the centre of the zeolite cavity and are not stabilized by H-bond interactions with oxygen atoms. Following this result, the fragment (6a) was selected as model of the H-Y zeolite cavity. The acidic hydrogen of this fragment not forming H-bonds was eliminated to simulate the presence of the contiguous acidic and nucleophilic centres on the oxygen atoms around one of the two Al atoms.

The optimized geometries of the two RRR and SRR epimers of the HMR species, in their most stable conformation, adsorbed within the H-Y cavity model, are shown in Fig. 7. The analysis of Fig. 7a and b reveals that both the HMR epimers may diffuse through the H-Y zeolite cavity in open conformation and then can be adsorbed over the H-Y inner surface, for example through the occurrence of H-bonds between one of the zeolite acidic hydrogen and the –OH12 oxygen, placed at ca. 200 pm irrespectively of the considered epimer. In this context, it is worth recalling that the benzylic oxygen is by far the most favored protonation site [14].

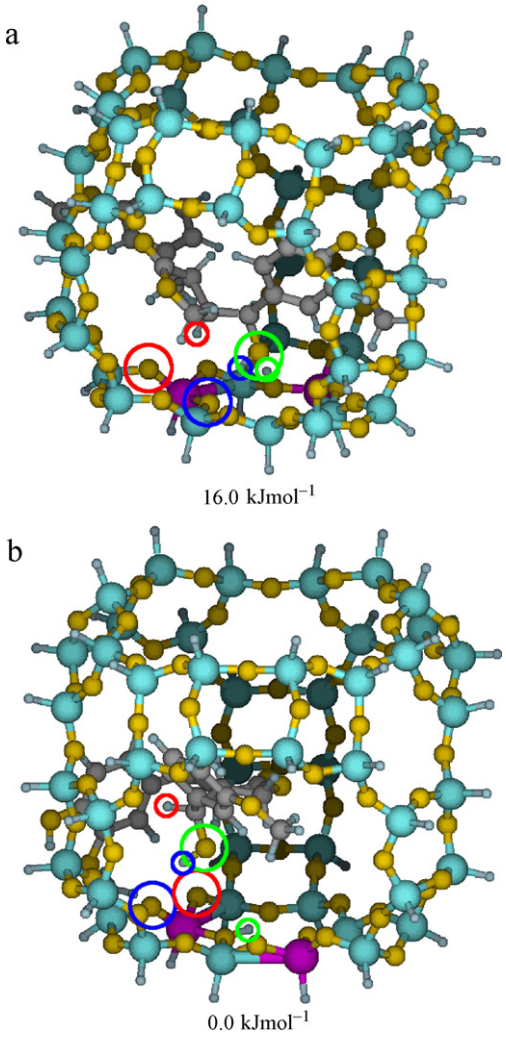

Fig. 7. Optimized structures of the SRR (a) and RRR (b) epimers of HMR in their most stable conformation, adsorbed within the di-aluminated Y cavity model; the circles individuate the different interaction centres, namely hydrogen (small circle) and oxygen (large circle) atoms, characterizing the H-Y fragment and the HMR epimers; in green are highlighted the interaction centres between the HMR –OH12 group and the zeolite acidic site, in blue those between the hydrogen of the HMR –OH12 group and one Al–O–Si oxygen site and finally in red those between the HMR H8 atom and the zeolite nucleophilic site; the relative DFT energy values are reported below the corresponding fragments.

In the SRR-HMR/H-Y system the β-hydrogen, H8 atom, also interacts at the same distance above with the nucleophilic oxygen atom bound to the Al centre (see Fig. 7a). This configuration is in this case possible because in the structure of the lowest energy minimum of the SRR species, both the β-hydrogen and the hydroxyl group, each other in *syn* conformation, point toward the zeolite surface. As a consequence vicinal nucleophilic and acidic groups of the same zeolite surface could simultaneously and easily activate the H8 atom and the –OH12 group toward the E2 elimination mechanism (i.e. following the proposed M2b pathway). Conversely, in the RRR-HMR/H-Y system the β-hydrogen and the hydroxyl group are in *anti* conformation and the substrate/catalyst interaction can occur only through the –OH12 group, being the HMR β-hydrogen at about 500 pm from the closest nucleophilic centre and pointing in the direction of the zeolite supercage (see Fig. 7b).

In this way, the HMR β-hydrogen is not activated together with the –OH12 group for a concerted β-elimination, hence the RRR isomer should be converted to the olephinic intermediate following the more complex E1 β-elimination (i.e. the M2a pathway). An

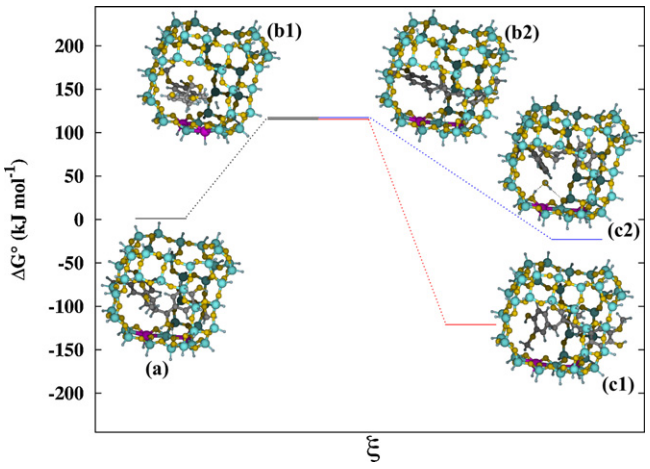

Fig. 8. Simplified (ΔG° vs. ξ) pathway representation (i) of the HMR protonation water-elimination route, giving the carbenium ionic species: (a)→(b2) black step, (ii) of the $H_2 \leftrightarrow H_2O$ exchange (see text), occurring close to the carbenium ionic species: (b2)→(b1) step, (iii) of the carbenium ionic species direct hydrogenation route, giving MAT: (b1)→(c1) red step, and (iv) of the carbenium ionic species deprotonation route, giving the olefinic intermediate: (b2)→(c2) blue step; (b1) and (b2) fragments differ for the presence of one H2 and one H_2O molecule – placed in the former and in the latter – in-between the carbenium species and the zeolite surface; the free energies corresponding to (b1) and (b2) fragments are arbitrarily posed to the same value (118 kJ mol^{-1}) whereas the values of both (b2) and (c2) and of (c1) are referred to those of (a) and (b1) fragments, respectively.

evident difficulty is indeed represented by the conversion of the carbenium species formed after water elimination. In this conversion, the carbenium-ion must desorb from the negatively charged surface and reabsorb with the atom H8 pointing at one nucleophilic centre. Taking into account the high energy that is required to accomplish the step above, it is reasonable to hypothesize that the conversion of the RRR-HMR epimer should essentially occur following the M1 mechanism.

Noteworthy, the SRR-HMR/H-Y system is less stable than the RRR-HMR/H-Y system by about 16 kJ mol^{-1}. Accordingly, the adsorption energy, calculated as the difference between the energy of the HMR/H-Y adducts and that of the corresponding isolated HMR + H-Y systems, resulted to be ca. −79 kJ mol^{-1} for SRR-HMR/H-Y and ca. −95 kJ mol^{-1} for RRR-HMR/H-Y, being the BSSE corrections not affecting the relative energy order. The stability of the RRR-HMR with respect of the SRR-HMR epimer could be explained, inferring that a smaller steric hindrance is present in the RRR-HMR/H-Y system. This is in agreement with the fact that SRR-HMR shows a larger number of interaction/activation points with the H-Y surface. The smaller number of activation points and the consequent larger adsorption stability of the RRR-HMR/H-Y could contribute to justify its experimentally observed lower reactivity [11], as explained below.

Fig. 8 following the black + blue steps' route, shows a simplified reaction pathway for the protonation β-elimination dehydration steps represented in Fig. 3, considering the SRR-HMR epimer. Negligible differences occur in the energetic path when the RRR-HMR epimer is involved. As already discussed, the kinetics involving E1 and E2 mechanisms for the RRR and SRR epimers should be, at variance with the corresponding energetics, very different. The relative energy values for the SRR epimeric system are reported in Table 1. The energy of the carbenium species calculated by the B3LYP method is at 98 kJ mol^{-1} compared to that of the adsorbed reactant. In this system, the eliminated water is adsorbed on the zeolite surface while the cationic species is moved toward the centre of the zeolite cavity (see (b2) in Fig. 8). The olefinic intermediate (see (c2) in Fig. 8) is conversely at 28 kJ mol^{-1} from the adsorbed reactant and interacts with the acidic hydrogen through the O14 carbonyl oxygen atom. The acidic hydrogen is the same atom previously released in the β-elimination step.

The optimized geometries obtained by the ONIOM method are almost undistinguishable from those obtained by the DFT-B3LYP method. Moreover, the trend of the B3LYP energy of the high-level is similar to that obtained by the B3LYP calculations on the whole system (see Table 1). Noteworthy, the standard free energy of the product, obtained by the ONIOM calculations, is lower than that of the reagent. Such result would indicate that a consistent entropic effect could play a role in the reaction outcome. Moreover, the analysis of the normal vibration modes suggests that the carbenium ion fragment originated by the HMR one, (b2) in Fig. 8, could even be a TS with an activation free energy of 118 kJ mol^{-1}. This species actually involves a reaction coordinate characterized by an imaginary vibration occurring along the line connecting the CH group and the coming out H_2O molecule, being the HC–OH_2 distance of ca. 220 pm.

The MP2 results, in principle able to account for the influence of dispersion effects inside the zeolite cavities [17,19] are also reported in Table 1. The behavior of the MP2 findings are qualitatively similar to those obtained either by the ONIOM or by the DFT methods, showing that the properties of the HMR molecules and derivatives, involved in the title reaction, are not largely affected by dipolar effects. In this context, it is interesting to notice that both the H_2O and H_2 molecules, when present, act as molecular-hooks – able to fix the organic molecules close to the inner surface of the zeolite fragments – and strongly affect the local arrangement of the molecules inside the H-Y cavity. This, in our opinion, supports the hypothesis of the existence of small dipolar effects exerted by the inner zeolite walls on the complex organic molecules of interest in the present work.

The simplified (ΔG° vs. ξ) pathway of Fig. 8, shows that the olefinic intermediate is energetically favored if compared with the carbenium ionic species hypothesized by Markus et al. on the basis of experimental evidences (M1 mechanism) [10]. The low free energy characterizing the olefinic intermediate (@ ca. −23 kJ mol^{-1} with respect to the HMR starting species) in our opinion confirms that the M1 and M2 mechanisms may concurrently take place. In order to evaluate the relative occurrence probability of the M1 and M2 mechanisms, a possible direct hydrogenation step starting by the carbenium ionic species and ending to MAT was searched (see red step pathway of Fig. 8). In this case, one H_2 substituted the H_2O molecule produced along the formation of the carbenium species.

Table 1
Relative energy values of the structures reported in Fig. 8, obtained by DFT(B3LYP), ONIOM(B3LYP/AM1) and MP2 calculations.

Energy difference[a] (kJ mol^{-1})	Fragment[b] (a)	Fragment (b1)	Fragment (b2)	Fragment (c1)	Fragment (c2)
ΔE_{dft}	0.0	–	98	–	28
ΔE_{oniom}	0.0	165	165	4	61
ΔE_{mp2}	0.0	109	109	−15	30
ΔG°	0.0	118	118	−111	−23

[a] Fragments (a), (b1), (b2), (c1) and (c2) respectively involve the HMR molecule, the carbenium ionic species either with water or hydrogen, the MAT molecule and the olefinic intermediate inside the H-Y fragment.
[b] ΔE_{oniom} reports the B3LYP energy difference calculated on the ONIOM model level while ΔE_{mp2} and ΔG° are calculated on the ONIOM optimized structures.

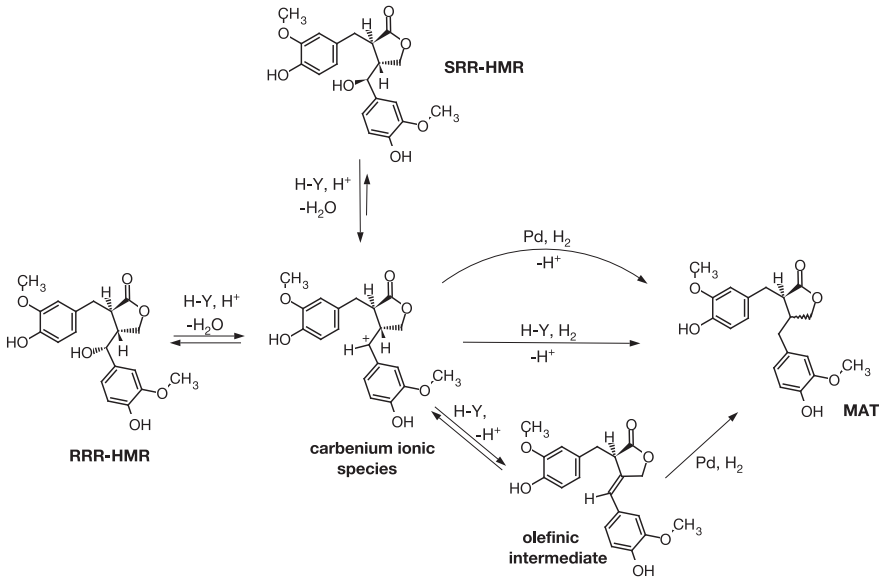

Fig. 9. Schematic representation of the HMR to MAT–M1 + M2–reaction mechanism: details on the different reactivity of the HMR epimers. The $-H^+$ terms, which are present in both the hydrogenation steps of the carbenium ionic species occurring over the zeolite (H-Y) and the metallic (Pd) component of the bi-functional catalyst, restore the acidic site on the zeolite inner surface or remain adsorbed on the palladium cluster.

The choice to pose at the same values the energetic parameters concerning the carbenium ionic species interacting both with the H_2 and H_2O is clearly an artifact and deserves explanations. In fact, the simulated title processes mimic experimental reactions conducted at chemical regime, where interphase and bulk diffusion effects are not affecting the reaction kinetics [39]. Since the $H_2O \leftrightarrow H_2$ exchange can be mostly regarded as the result of diffusion events, the corresponding carbenium-ion/H-Y fragments involving either molecular hydrogen or water were here considered as each other independent and the molecular $H_2O \leftrightarrow H_2$ local exchange, occurring inside the zeolite cavity, not influential on the reaction rate. Following these inferences and for simplicity of representation, the two fragments above were therefore placed at the same differential energetic values.

Noteworthy, we have not found any other intermediates or TS species between the carbenium-ion and MAT, being the latter interacting with the re-protonated zeolite at ca. $-229\,kJ\,mol^{-1}$ with respect to the former. As clearly shown by Fig. 8, within the zeolite cavity, MAT is more stable than the olefinic intermediate, if the energetics of both systems are relative to that of the starting carbenium-ion. The absence of a TS species, in the red step pathway, would confirm the character of transition state – already inferred for the carbenium ionic species – while the large stability of the MAT fragment with respect to the olefinic intermediate would suggest that M1 is the preferred reaction mechanism. However, the occurrence of the M1 mechanism, as represented in Fig. 2, does not apparently allow to discriminate between the different reactivity of the two epimers.

Conversely, in the parallel M2 mechanism the transformation of the RRR and SRR species to the olefinic intermediate could respectively occur *via* the M2a and M2b paths, thereby discriminating between the epimer conversion rate. The following hydrogenation of the olefinic intermediate over palladium should mostly occur in *syn* (with respect to the Pd/H-Y catalyst surface) hence should produce only the RR-MAT species, as experimentally found.

Nevertheless, the observed different reactivity of the two epimers could be driven by the isomerization of SRR-HMR to RRR-HMR. The latter, experimentally pointed out on several catalysts and namely on the palladium/zeolite catalytic systems [10], could be related to the back-way processes, characterizing both M1 and M2 mechanisms (see Fig. 9).

The SRR and RRR epimers could actually be interconverted by the reverse steps involved in the hydrogenolysis mechanisms. Despite that, two main reasons should favor the transformation of the SRR to the RRR species, also causing temporary accumulation of the latter along the title reaction [9,10]. In fact, due to the easier activation by the zeolite surface of the SRR epimer, we could expect that the latter generates the RR carbenium derivative more frequently than the RRR epimer.

As a consequence, the SRR epimer should undergo either hydrogenation or isomerization more frequently than the RRR epimer. In addition, due to steric hindrance reasons, the back protonation water-addition steps, restoring the HMR molecules form the already produced olefinic intermediate, should occur with higher probability by an *anti* addition (giving RRR epimer) than a *syn* addition (giving SRR epimer).

The first point is clearly at the basis of the larger reactivity of the SRR epimer already discussed. Whereas, the second point, straightforwardly connected with the SRR to RRR isomerization mechanism, is easily understandable considering that the proton species should originate from the zeolite surface while water molecule very likely by diffusion processes, occurring through the zeolite cavities.

These considerations allow us to infer the existence of an integrated reaction process, including both M1 and M2 mechanisms, as represented in Fig. 9. The asymmetry in the double arrows, characterizing the back protonation water-addition step of the carbenium-ion to form the SRR-HMR epimer, underlines the smaller probability that characterizes this process with respect to the one, driving to the RRR-HMR formation.

Fig. 9 also illustrates a hypothesized hydrogenation step occurring on palladium, which starting by the carbenium-ion directly originates MAT. A minimal $2H/Pd_2$ cluster model was used to test this reaction pathway, being the results illustrated in the up frame (A box) of Fig. 10.

Despite the use of a very approximate model of Pd cluster, some interesting aspects of the role of the metal in the bi-functional catalyst can be drawn. In fact, comparing the energetics involved in the carbenium hydrogenation processes over zeolite (see Fig. 8) and palladium (see Fig. 10), schematized in Fig 9 as H-Y and Pd pathways, distinctly appears the barely subordinate role of the metallic function in reducing the carbenium species. Indeed, at variance

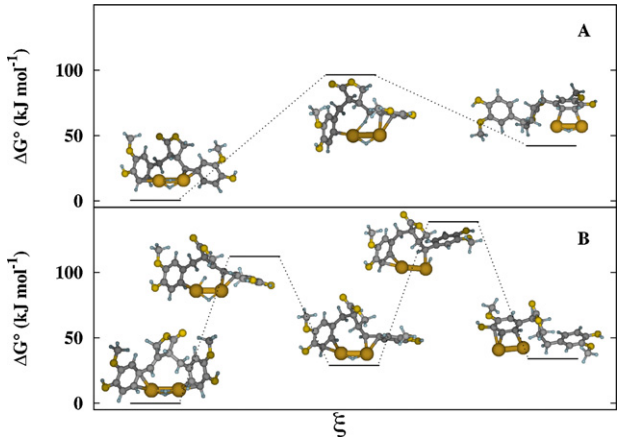

Fig. 10. Reaction pathway (ΔG° vs. ξ) characterizing the hydrogenation of the carbenium-ion ($\Delta G^\circ = 0$ in A box) and olefinic intermediate species ($\Delta G^\circ = 0$ in B box) to MAT.

with the not activated hydrogenation occurring on H-Y the corresponding process on palladium is not only activated (TS @ ca. 92 kJ mol^{-1}) but the product is also less stable (43 kJ mol^{-1}) than the reactant. The latter effect could in part be attributed to the small size of the Pd cluster used, or to the residual H^+ ion placed on the palladium cluster and could be probably minimized by a migration, in any case difficult [20], of the protonic species on nucleophilic oxygens present on the zeolite surface.

The consideration of the equilibrium mechanisms reported in Fig. 9 could help to understand the role of the local acidity when the palladium/zeolite bi-functional catalysts are used. As already recalled, in the title hydrogenolisys the Brønsted acidity is in fact necessary to start the reaction but the catalyst activity decreases as the number of the same Brønsted acidic sites increases. This peculiar behavior could be caused by two opposite effects related to the relevance on the whole mechanism of the isomerization processes and of the olefinic intermediate formation. These are in fact activated by a protonation step (to form the carbenium-ion) that is favored by the acidic sites' presence but are closed either by a deprotonation water-addition step (to form the HMR species) or by a deprotonation water-elimination step (to form the olefinic intermediate) that are inhibited by acidic sites.

As already stated, after the β-elimination step and following the M2 mechanism, both the HMR isomers converge to the same olefinic intermediate, having R chirality. The latter, in a bi-functional catalyst, can be reduced to MAT over Pd aggregates by a two-step mechanism. The simulated reduction pathway of the olefinic intermediate over the minimal $2H/Pd_2$ cluster model is shown in the down frame (B box) of Fig. 10.

In the reduction pathway above, hydrogen migration should occur from the palladium cluster to the olefinic intermediate. The transition states of the two-step reduction mechanism are characterized by activation energies (ca. 110 and ca. 135 kJ mol^{-1}) that are accessible at the experimental conditions in which the reaction is usually carried out [10]. Therefore, hypothesizing the olefinic intermediate formation, a supportive role of the M2 mechanism in the MAT production over bi-functional catalysts could be also inferred. Moreover, the presence of the metal inside the zeolite cavities, in the presence of adsorbed hydrogen, can modify the local acidity of the zeolite [20].

As a matter of fact, the last steps of all possible reaction pathways leading to MAT, collectively reported in Fig. 9, involve: (i) the hydrogenation of the carbenium ion, catalyzed by the H-Y zeolite or by the Pd metal, or (ii) the hydrogenation of the olefinic intermediate, catalyzed by the Pd metal.

It is important to highlight that the latter process cannot be related to reaction rate-determining steps, because the olefinic intermediate hydrogenation over palladium involves HMR derivatives that have already lost the chirality at the epimeric centre C7. As such, this step cannot explain the higher reactivity of SRR-HMR compared to RRR-HMR. This hypothesis is *a fortiori* valid whenever the activation energy of the Pd catalyzed hydrogenation would result lower than that obtained by using the extremely simplified model of Pd metal cluster. On the other hand, the results of our calculations show: (i) that the energy barrier found in the M1 mechanism (see Fig. 8) is of the same order of magnitude of those found in the reduction steps catalyzed by Pd (see Fig. 10) and (ii) that the hydrogenation of the carbenium ion catalyzed by H-Y presumably occurs without activation energy.

These considerations lead us to conclude that the rate-determing steps, driving the selectivity in the HMR to MAT hydrogenolysys on Pd/H-Y catalysts, depend: (i) on the interconversion of SRR-HMR to RRR-HMR, occurring through the conversion of both epimers to the carbenium ionic species, and presumably to a very less extent (ii) by the interconversion of the latter with the olefinic intermediate, being both the interconversions above not involving palladium.

4. Conclusions

The present computational study allowed us to state that hydrogenolysis of hydroximatairesinol to give matairesinol may occur over bi-functional catalysts, namely over Pd/H-Y catalysts, following different mechanisms both starting from the RRR-HMR and SRR-HMR epimers. These mechanisms can be distinguished either for the direct participation in the final hydrogenation step of the metallic function or for the apparent absence of role of the same catalytic metal component. Confirming the experimental findings, the computational results show that a composite mechanism in which the metal function plays a minor role is the most favorite process.

On the whole, the present computational study was able to point out details on the reaction pathways, to rationalize the different reactivity, experimentally observed, between the RRR-HMR and SRR-HMR epimers, and to give hints on the role of the acidity on the title hydrogenolysis.

The results finally confirm the importance of the conformational analysis in describing the substrate/catalyst interactions and in explaining the consequent reactivity of the adsorbed substrate derivatives. It is moreover possible to hypothesize that the analysis of the conformational space of HMR, and of its derivatives, within the H-Y cavity could be of help in order to achieve an even clearer picture of the title system.

Acknowledgements

This work is an extension of the NanoCat Project, funded in the frame of the 6th Framework Programme of the European Community: Contract No. NMP3-CT-2005-506621. The work was also supported by the University of Palermo and the Italian Ministero dell'Università e della Ricerca. Calculations were run on the CCCP Linux cluster, close to the Department of Inorganic and Analytical Chemistry "S. Cannizzaro" of the University of Palermo and on the COMETA HPC cluster, close to the Department of Physics and Astronomy of the University of Palermo.

References

[1] M. Axelson, J. Sjövall, B.E. Gustafsson, K.D.R. Setchell, Nature 298 (1982) 659–660.

[2] N.M. Saarinen, R. Huovinen, A. Wärri, S.I. Mäkelä, L. Valentín-Blasini, R. Sjöholm, J. Ämmälä, R. Lehtilä, C. Eckerman, Y.U. Collan, R.S. Santti, Mol. Cancer Ther. 1 (2002) 869–876.
[3] A. Bylund, N. Saarinen, J.X. Zhang, A. Bergh, A. Widmark, A. Johansson, E. Lundin, H. Adlercreutz, G. Hallmans, P. Stattin, S. Mäkelä, Exp. Biol. Med. 230 (2004) 217–223.
[4] R. Ekman, Acta Acad. Abo. B 39 (3) (1979) 1–6.
[5] B. Holmbom, C. Eckerman, P. Eklund, J. Hemming, L. Nisula, M. Reunanen, R. Sjöholm, A. Sundberg, K. Sundberg, S. Willför, Phytochem. Rev. 2 (2003) 331–340.
[6] S. Willför, J. Hemming, M. Reunanen, C. Eckerman, B. Holmbom, Holzforschung 57 (2003) 27–36.
[7] J. Mattinen, R. Sjöholm, R. Ekman, ACH Models Chem. 135 (1998) 583–590.
[8] P Eklund, R. Sillanpää, R. Sjöholm, J. Chem. Soc. Perkin Trans. I 16 (2002) 1906–1910.
[9] P. Eklund, A. Lindholm, J.-P. Mikkola, A. Smeds, R. Lehtilä, R. Sjöholm, Org. Lett. 5 (4) (2003) 491–493.
[10] H. Markus, P. Mäki-Arvela, N. Kumar, N.V. Kul'kova, P. Eklund, R. Sjöholm, B. Holmbom, T. Salmi, D.Y. Murzin, Catal. Lett. 103 (2005) 125–131.
[11] H. Markus, P. Mäki-Arvela, N. Kumar, T. Heikkilä, V.-P. Lehto, R. Sjöholm, B. Holmbom, T. Salmi, D.Y. Murzin, J. Catal. 238 (2006) 301–308.
[12] H. Markus, A.J. Plomp, P. Mäki-Arvela, J.H. Bitter, D.Y. Murzin, Catal. Lett. 113 (2007) 141–146.
[13] H. Markus, P. Mäki-Arvela, N. Kumar, T. Salmi, D.Y. Murzin, Catal. Today 121 (2007) 101–105.
[14] G. Li Manni, G. Barone, D. Duca, D.Y. Murzin, J. Phys. Org. Chem. 23 (2010) 141–147.
[15] G. Barone, G. Casella, S. Giuffrida, D. Duca, J. Phys. Chem. C 111 (2007) 13033–13043.
[16] V. Nieminen, M. Sierka, D.Y. Murzin, J. Sauer, J. Catal. 231 (2005) 393–404.
[17] C. Tuma, J. Sauer, Phys. Chem. Chem. Phys. 8 (2006) 3955–3965.
[18] I. Milas, M.A.C. Nascimento, Chem. Phys. Lett. 418 (2006) 368–372.
[19] S. Svelle, C. Tuma, X. Rozanska, T. Kerber, J. Sauer, J. Am. Chem. Soc. 131 (2) (2009) 816–825.
[20] G. Barone, N. Armata, A. Prestianni, T. Rubino, D. Duca, D.Y. Murzin, J. Chem. Theory Comput. 5 (2009) 1274–1283.
[21] N. Armata, G. Baldissin, G. Barone, R. Cortese, V. D'Anna, F. Ferrante, S. Giuffrida, G. Li Manni, A. Prestianni, T. Rubino, D. Duca, Top. Catal. 52 (2009) 444–455.
[22] R.A. van Santen, J. Mol. Catal. A: Chem. 115 (1997) 405–419.
[23] A. Aho, N. Kumar, A. Lashkul, K. Eränen, M. Ziolek, P. Decyk, T. Salmi, B. Holmbom, M. Hupa, D.Y. Murzin, Fuel 89 (2010) 1992–2000.
[24] M.J. Frisch, G.W. Trucks, H.B. Schlegel, G.E. Scuseria, M.A. Robb, J.R. Cheeseman, J.A. Montgomery Jr., T. Vreven, K.N. Kudin, J.C. Burant, J.M. Millam, S.S. Iyengar, J. Tomasi, V. Barone, B. Mennucci, M. Cossi, G. Scalmani, N. Rega, G.A. Petersson, H. Nakatsuji, M. Hada, M. Ehara, K. Toyota, R. Fukuda, J. Hasegawa, M. Ishida, T. Nakajima, Y. Honda, O. Kitao, H. Nakai, M. Klene, X. Li, J.E. Knox, H.P. Hratchian, J.B. Cross, V. Bakken, C. Adamo, J. Jaramillo, R. Gomperts, R.E. Stratmann, O. Yazyev, A.J. Austin, R. Cammi, C. Pomelli, J.W. Ochterski, P.Y. Ayala, K. Morokuma, G.A. Voth, P. Salvador, J.J. Dannenberg, V.G. Zakrzewski, S. Dapprich, A.D. Daniels, M.C. Strain, O. Farkas, D.K. Malick, A.D. Rabuck, K. Raghavachari, J.B. Foresman, J.V. Ortiz, Q. Cui, A.G. Baboul, S. Clifford, J. Cioslowski, B.B. Stefanov, G. Liu, A. Liashenko, P. Piskorz, I. Komáromi, R.L. Martin, D.J. Fox, T. Keith, M.A. Al-Laham, C.Y. Peng, A. Nanayakkara, M. Challacombe, P.M.W. Gill, B. Johnson, W. Chen, M.W. Wong, C. Gonzalez, J.A. Pople, Gaussian 03 Revision D.02, Gaussian, Inc., Wallingford, CT, 2005.
[25] C. Baerlocher, W.M. Meyer, D.H. Olson, Atlas of Zeolite Framework Types, 5th Edition, Elsevier, Amsterdam, 2001.
[26] Database of zeolite structures, URL: http://www.iza-structure.org/databases/ (accessed 21.01.09).
[27] Database of zeolite structures, zeolite framework types, URL: http://izasc.ethz.ch/fmi/xsl/IZA-SC/ft.xsl (accessed 21.01.09).
[28] W. Loewenstein, Am. Miner. 39 (1954) 92–96.
[29] M. Svensson, S. Humbel, R.D.J. Froese, T. Matsubara, S. Sieber, K. Morokuma, J. Phys. Chem. 100 (1996) 19357–19363.
[30] S. Dapprich, I. Komároni, K. Byun, K. Morokuma, M.J. Frisch, J. Mol. Struct. (Theochem) 461/462 (1999) 1–21.
[31] M.J.S. Dewar, E.G. Zoebisch, E.F. Healy, J.J.P. Stewart, J. Am. Chem. Soc. 107 (13) (1985) 3902–3909.
[32] J.B. Foresman, A. Frisch, Exploring Chemistry with Electronic Structure Methods, 2nd Edition, Gaussian Inc., Pittsburgh, PA, 1996.
[33] C. Møller, M.S. Plesset, Phys. Rev. 46 (1934) 618–622.
[34] M. Head-Gordon, J.A. Pople, M.J. Frisch, Chem. Phys. Lett. 153 (1988) 503–506.
[35] S. Saebø, J. Almlöf, Chem. Phys. Lett. 154 (1989) 83–89.
[36] M.J. Frisch, M. Head-Gordon, J.A. Pople, Chem. Phys. Lett. 166 (1990) 275–280.
[37] M.J. Frisch, M. Head-Gordon, J.A. Pople, Chem. Phys. Lett. 166 (1990) 281–289.
[38] C. Peng, P.Y. Ayala, H.B. Schlegel, M.J. Frisch, J. Comput. Chem. 17 (1996) 49–56.
[39] J.R. Madon, M. Boudart, Ind. Eng. Chem. Fundam. 21 (1982) 438–447.